ELSEVIER

Solid State Ionics 149 (2002) 299–307

SOLID STATE IONICS

www.elsevier.com/locate/ssi

Transport and surface properties of $Sr_{0.25}Bi_{0.5}FeO_{3-\delta}$ mixed conductor

Xinyu Lu, Meilin Liu*

School of Materials Science and Engineering, Georgia Institute of Technology, Atlanta, GA 30332-0245, USA

Received 13 December 2001; received in revised form 8 April 2002; accepted 24 April 2002

Abstract

The ionic and electronic conductivities and surface properties of a perovskite-type oxide, $Sr_{0.25}Bi_{0.5}FeO_{3-\delta}$ (SBF), are studied using impedance spectroscopy and gas permeation measurements. SBF is a promising cathode material for intermediate-temperature solid oxide fuel cells (SOFCs) and has a good potential to be used as a membrane material for methane conversion. The ionic conductivities and the interfacial resistances are determined from the dependence of oxygen permeation rate on membrane thickness, which are further confirmed from the dependence of oxygen permeation rate on the partial pressure of oxygen. Results suggest that the interfacial resistances limit the oxygen permeation rates in the temperature range studied (700–800 °C) at low partial pressures of oxygen.

Keywords: Ceramic membrane; Mixed conductor; Ionic conductivity; Oxygen permeation; Interfacial resistance

1. Introduction

Mixed ionic–electronic conductors (MIECs) play an important role in many solid-state electrochemical devices (such as gas sensors, batteries, and fuel cells) and processes (such as fuel processing and gas separation) [1,2]. For example, the ambipolar diffusion of oxygen through a dense MIEC membrane, as a consequence of simultaneous transport of both ionic and electronic charge carriers under the influence of a gradient in partial pressure of oxygen, can be used for oxygen separation. However, the permeation of oxygen through a dense MIEC membrane involves two processes, the surface exchange reactions at the gas/MIEC interfaces and the ambipolar transport through the bulk membrane. For a thin MIEC membrane with high oxygen ion conductivities, the surface exchange reactions could become the rate-limiting step in oxygen permeation [3,4]. MIECs can be a multi-phase composite or single-phase (homogeneous) oxide, such as fluorites (e.g., CeO_2), pyrochlores (e.g., $Gd_2Ti_2O_7$), and traditional perovskites (e.g., $LaCoO_3$-based compositions) [5]. Perovskite-type mixed conductor, $Sr_{0.25}Bi_{0.5}FeO_{3-\delta}$ (SBF), appears to have superior ionic and electronic conductivities, good chemical and thermal stability, and high catalytic activity for oxygen reduction [6,7]. SBF is considered to be a promising cathode material for intermediate-temperature solid oxide fuel cells (SOFCs) [6] and a potential membrane material for methane conversion [7]. The use of an MIEC as electrode may reduce the polar-

* Corresponding author. Tel.: +1-404-894-6114; fax: +1-404-894-9140.

E-mail address: meilin.liu@mse.gatech.edu (M. Liu).

0167-2738/02/$ - see front matter
PII: S0167-2738(02)00277-1

ization losses due to the extension of active electrochemical reaction sites from the triple-phase boundary (TPB) to the surface of the MIEC electrode. In the case of methane conversion, the use of MIEC membranes may integrate oxygen separation, steam reforming, and partial oxidation of methane into a one-step process [8,9], eliminating not only a costly oxygen plant but also the generation of harmful pollutants (NO_x).

The objective of this study is to separate the ionic from the electronic transport properties of $Sr_{0.25}Bi_{0.5}FeO_{3-\delta}$ in order to further improve its properties for better performance in oxygen permeation and electrocatalysis. The interfacial resistances were separated from the bulk resistance by the dependence of the oxygen permeation rate on membrane thickness and on the partial pressure of oxygen.

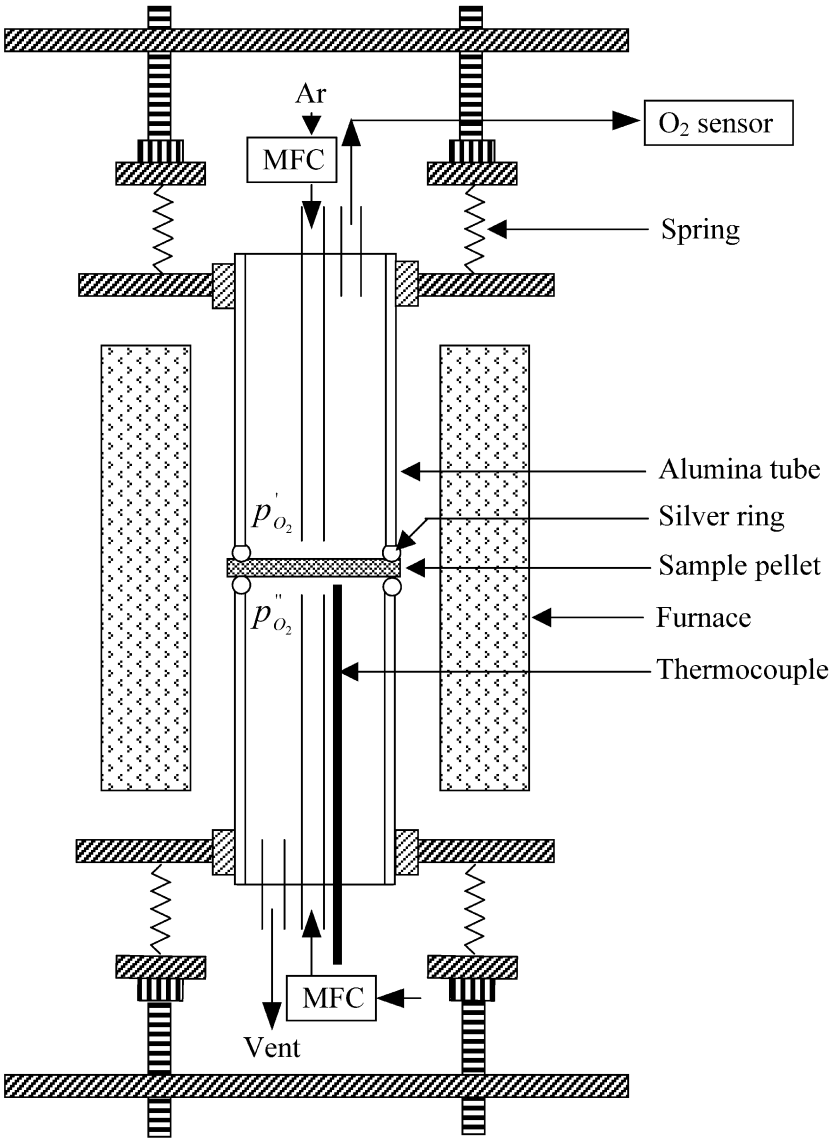

Fig. 1. A schematic experimental setup for oxygen permeation measurements.

2. Experimental

$Sr_{0.25}Bi_{0.5}FeO_{3-\delta}$ was prepared using a solid-state reaction method as described previously [7]. The microstructures of the sintered samples were examined using a scanning electron microscope (SEM, Hitachi S-800). Schematically shown in Fig. 1 is the home-built set-up for gas permeation measurements. The SBF pellet was sealed between two spring-forced alumina tubes using silver rings. In order to secure the sealing, the ends of the alumina tubes and both sides of the silver ring and the SBF pellet were grinded and polished. Further, all SBF samples were taken from the same batch and all surfaces were prepared under the same conditions in order to minimize the variation in surface properties from sample to sample. The final thicknesses of the SBF pellets (1.60 cm in diameter) varied from 0.040 to 0.104 cm.

Argon (Air Products: 99.998%) was used as the carrier gas throughout the gas permeation measurements. The residue oxygen content in the carrier gas was about 1.4×10^{-5} atm, as determined using an oxygen sensor based on yttria-stabilized zirconia (YSZ). Air (Air Products: breathing quality) and 0.995% O_2 balanced with N_2 (Air Products) were used to make gas mixtures containing 1%, 5%, and 21% of oxygen. Oxygen (Air Products: 99.8%) was also used in gas permeation measurements and in determining the total electrical conductivity of the SBF samples. A gas chromatograph (Varian 3800) was used to monitor the leakage by checking the existence of the N_2 peak on the permeate side. The flow rates of all gases and gas mixtures were controlled by mass flow controllers (MFCs). The flow rate was always kept constant (35.3 ml·min^{-1}) on the permeate side, since the oxygen permeation rate is very sensitive to gas flow rate. On the feed side, the flow rate was kept at 40.0 ml·min^{-1}. The oxygen permeation rates were measured at temperatures from 700 to 800 °C. For thickness dependence measurements, the partial pressure of oxygen was kept at 0.21 atm on the feed side and 1.4×10^{-5} atm on the permeate side. To measure the dependence of oxygen permeation rate on partial pressure of oxygen, oxygen partial pressure was changed from 0.01 to 1 atm on the feed side and maintained constant at 1.4×10^{-5} atm on the permeate side. It typically took about 30 min to 1 h for the system to reach a steady state when the temperature or the oxygen partial pressure was changed for each measurement.

The currents due to the motion of ionic defects through the SBF membranes (pellets) were calculated from the observed molar flux of oxygen as follows [10],

$$j_{O^{2-}} = 78.38(v_2x_2 - v_1x_1)/T_1 \quad (1)$$

where v_1 and v_2 are the volume flow rates (cm^3/min) of the incoming and the outgoing gas stream, respectively, as measured at room temperature (T_1) in Kelvin, whereas x_1 and x_2 are the molar fraction of

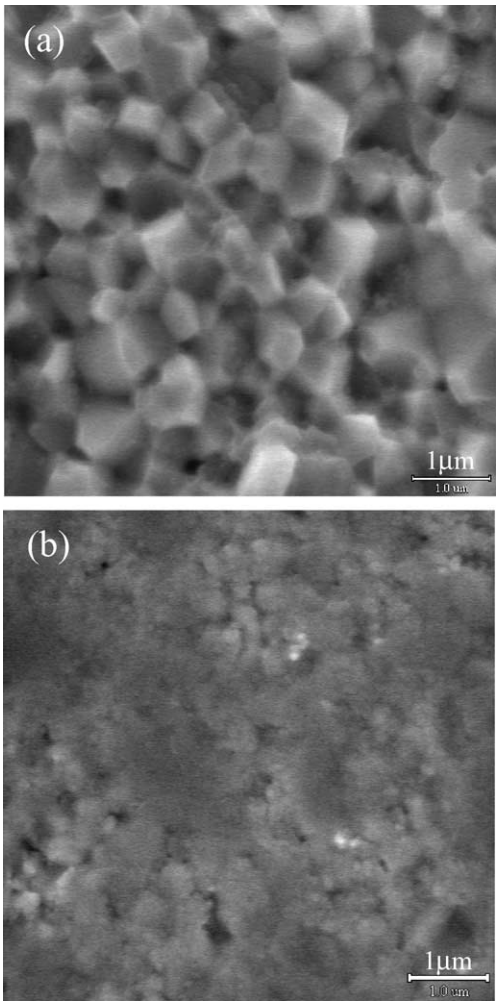

Fig. 2. SEM micrographs of an as-polished SBF pellet: (a) a cross-sectional view and (b) a top view of the polished surface.

oxygen in the incoming and the outgoing gas stream, respectively, which were determined using a YSZ-based oxygen sensor.

A bar sample (with dimension of $0.080 \times 0.40 \times 1.46$ cm^3) of SBF was used to measure the total electrical conductivities in a uniform atmosphere at different temperatures using impedance spectroscopy. An EG&G lock-in amplifier (5201) and an EG&G potentiostat/galvanostat (273A), interfaced with a computer, were used for impedance measurements in the frequency range from 10^{-2} Hz to 100 kHz. The resistance of the lead wires was carefully removed in the measurements.

3. Results and discussion

3.1. Microstructures of the SBF samples

Shown in Fig. 2 are a cross-sectional view and a top view of an as-polished SBF pellet. Both surface and cross-sectional views show that the grain size of the SBF is about 1 μm with narrow size distribution. The relative density of the SBF sample is about 95% of the theoretical value (impermeable to molecular gases). The surface is relatively smooth, and the surface microstructure and morphology are repeatable from sample to sample. XRD analysis indicates that the SBF has an orthorhombic structure with $a = 11.705$, $b = 19.195$, and $c = 5.513$ [11].

3.2. Dependence of oxygen permeation rate on membrane thickness (L)

Shown in Fig. 3 are the plots of $E_N/j_{O^{2-}}$ as a function of membrane thickness (L) at temperatures from 700 to 800 °C with an interval of 25 °C. In these permeation measurements, air and argon were used as the feed gas and the carrier gas, respectively, and the Nernst potential (E_N) across the SBF membranes,

$$E_N = \left(\frac{RT}{4F}\right)\ln\left(\frac{p_{O_2}''}{p_{O_2}'}\right) \quad (2)$$

remained constant for all thicknesses, where p_{O_2}' and p_{O_2}'' are the partial pressures of oxygen on the permeate side and on the feed side, respectively.

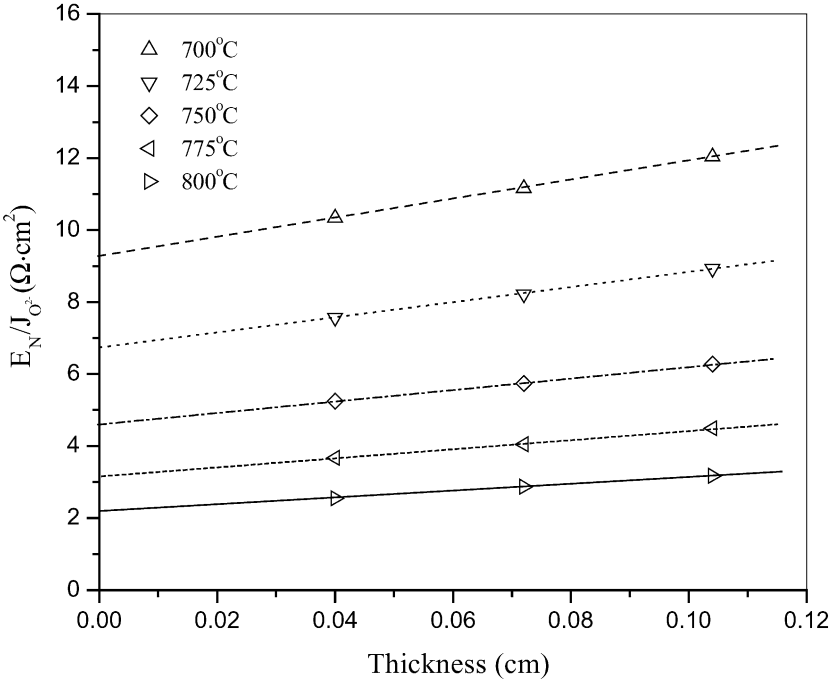

Fig. 3. Oxygen permeation versus the thickness of the SBF pellets at different temperatures.

Table 1
The ambipolar conductivities and the interfacial resistances from the thickness dependence measurements

T (°C)	700	725	750	775	800
$\sigma_{amb.}$ (S·cm^{-1})	0.03763	0.04704	0.06209	0.07761	0.1018
R_p (Ω·cm^2)	9.266	6.707	4.596	3.144	2.156

The ambipolar conductivities of the MIEC membranes were determined from the slope of the plot of $E_N/j_{O^{2-}}$ versus the membrane thickness (L) at a constant Nernst potential as

$$\sigma_{amb.} = \left[\frac{\partial(E_N/j_{O^{2-}})}{\partial L}\right]^{-1} \quad (3)$$

For an MIEC whose electronic conductivity is much greater than the ionic conductivity ($\sigma_{e^-} >> \sigma_{O^{2-}}$), the ambipolar conductivity is approximately equal to the ionic conductivity (i.e.,$\sigma_{amb.} \approx \sigma_{O^{2-}}$). The interfacial polarization resistances, R_p, were estimated from the intercepts of the plots as

$$R_p = \left(\frac{E_N}{j_{O^{2-}}}\right)_{L\to 0} \quad (4)$$

The oxygen ion fluxes ($j_{O^{2-}}$) increased with temperature for all SBF samples of different thicknesses. As implied by Eqs. (3) and (4), the ambipolar conductivities can be determined from the slopes of the plots, whereas the interfacial resistances can be obtained directly from the intercepts of the linear plots at the vertical axis (when extrapolated to the zero thickness) (Table 1). For each thickness, the subtraction of the interfacial resistance from each datapoint gives the bulk resistance (R_b) of the membrane. All SBF membranes displayed significant interfacial resistances ($R_b \ll R_p$) in the temperature range studied. As shown in Fig. 4, the activation energies are 87.3, 85.5, and 86.8 kJ·mol^{-1} for SBF pellets of thickness 0.040, 0.072, and 0.104 cm, respectively (the activation energies are within 5% of each other).

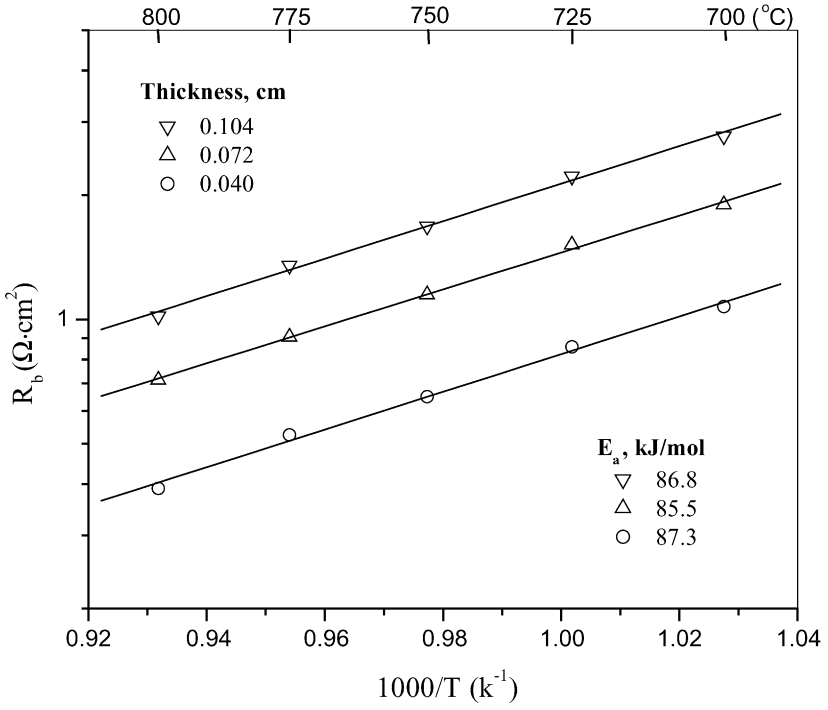

Fig. 4. Bulk resistances of the SBF samples with different thickness (0.040, 0.072, and 0.104 cm) as a function of temperature.

3.3. Total conductivities of the SBF samples

Shown in Fig. 5 are the total electrical conductivities (σ_T) of the SBF samples as determined in air and in O_2 at different temperatures, together with the ambipolar conductivities calculated from Fig. 3. The total electrical conductivity values in O_2 are greater than those in air, indicating that the SBF exhibits p-type conduction. This can be explained as follows. The substitution of Bi by Sr produces oxygen vacancies and the incorporation of O_2 into Sr-doped $BiFeO_3$ results in electron holes. The defect reactions may be expressed, using Kröger–Vink notation, as

$$2SrO \xrightarrow{Bi_2O_3} 2Sr_{Bi}' + 2O_O^{\times} + V_O^{\cdot\cdot} \quad (5)$$

$$V_O^{\cdot\cdot} + 1/2O_2 \rightarrow O_O^{\times} + 2h^{\cdot} \quad (6)$$

Since the ambipolar conductivities are about 1 to 2 orders of magnitude lower than the total electrical conductivities, the electronic conductivities are much greater than the ionic conductivities. In this case, the measurement of the oxygen permeation flux across the SBF pellet is the key for the calculation of ionic conductivity. At 800 °C, the oxygen ionic conductivity of the SBF is about 0.102 $S \cdot cm^{-1}$, which is close to that of $Sr_{0.9}Ce_{0.1}CoO_{3-\delta}$ (0.15 $S \cdot cm^{-1}$ at 800 °C) and even higher than that of YSZ [12] at 800 °C. The oxygen ion conduction in SBF depends strongly on temperature because the activation energy for oxygen ion conduction (86.5 $kJ \cdot mol^{-1}$) is much greater than those for total electrical conduction (35.6 and 53.2 $kJ \cdot mol^{-1}$). Shown in Fig. 6 are the transference numbers of oxygen ion, as calculated from the data shown in Fig. 5.

3.4. Dependence of $j_{O^{2-}}$ on p_{O_2}''

When an MIEC membrane is exposed to a chemical potential gradient and the external circuit is open, the dependence of the ionic current density (A/cm^2)

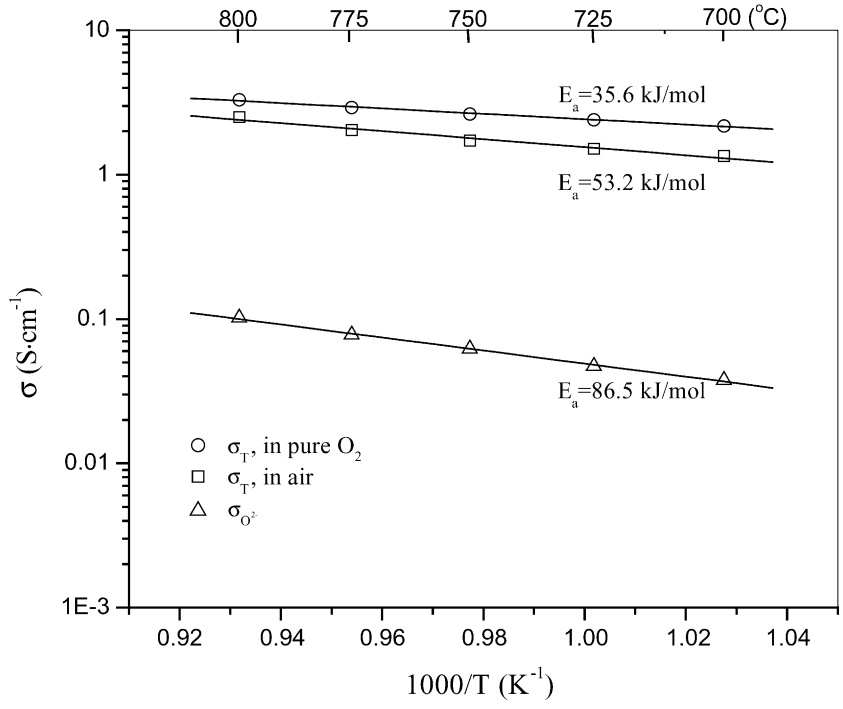

Fig. 5. Oxygen ion conductivities obtained from the thickness dependence measurements (Fig. 3) and total electrical conductivities determined from impedance measurements in air and oxygen.

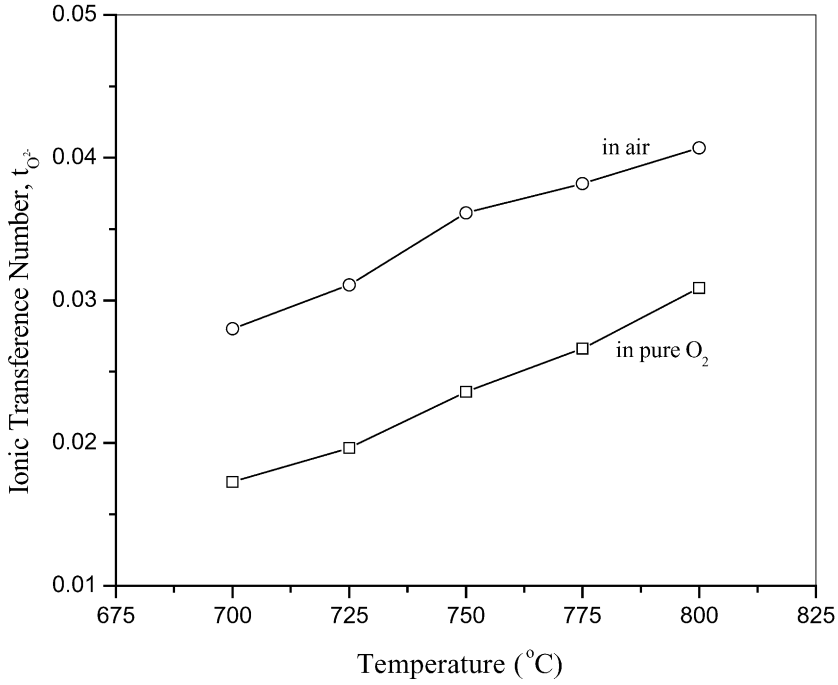

Fig. 6. Oxygen ion transference numbers determined from the data shown in Fig. 5 at different temperatures.

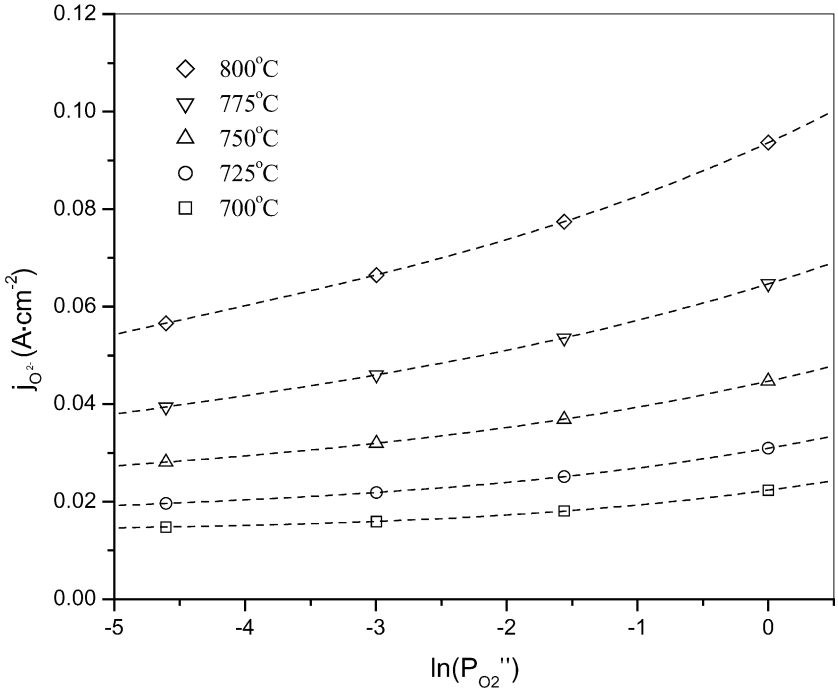

Fig. 7. Ionic current density versus the partial pressure of oxygen on the feed side at different temperatures (thickness of the SBF pellet was 0.072 cm).

on the partial pressure of oxygen (P_{O_2}'') can be described as [5]

$$\left[\frac{\partial j_{O^{2-}}}{\partial\left(\ln P_{O_2}''\right)}\right]_{L,P_{O_2}'} = \left(\frac{RT\sigma_{amb.}}{4FL}\right)\left(\frac{1}{1+\frac{R_p\sigma_{amb.}}{L}}\right) \tag{7}$$

where $\sigma_{amb.}$ is the ambipolar conductivity, which is given by

$$\sigma_{amb.} = \frac{\sigma_{O^{2-}}\sigma_{e^-}}{\sigma_{O^{2-}}+\sigma_{e^-}} \tag{8}$$

For SBF, $\sigma_{amb.} \approx \sigma_{O^{2-}}$ since $\sigma_e \gg \sigma_{O^{2-}}$. Shown in Fig. 7 are ionic current densities ($j_{O^{2-}}$) as a function of the partial pressure of oxygen (P_{O_2}'' as in Eq. (2)) at different temperatures. The partial pressure of oxygen on the feed side has more influence on the change of the interfacial resistance than that of the ionic conductivity. Here, the ionic conductivity was assumed constant (using $\sigma_{O^{2-}}$ from the thickness dependence measurements) as the partial pressure of oxygen was changed. Then, the interfacial resistances for different partial pressures of oxygen on the feed side can be calculated using Eq. (7) after the cubic polynomial fits were made in Fig. 7. Shown in Fig. 8 are the interfacial resistances determined from the dependence on partial pressure of oxygen and on membrane thickness, respectively. Although errors in these measurements are inevitable, the results show a clear tendency: the interfacial resistance increases as the partial pressure of oxygen on the feed side is reduced. Accordingly, the overall oxygen transport process was dominated by the interfacial resistances, especially for thin samples at lower operating temperatures and lower partial pressures of oxygen on the feed side. As temperature increases, the partial pressure of oxygen on the feed side has less influence on the interfacial resistance. The differences between the interfacial resistances determined from the thickness dependence measurements ($P_{O_2}'' = 0.21$) and those determined from the oxygen partial pressure measurements ($P_{O_2}'' = 0.21$) are less

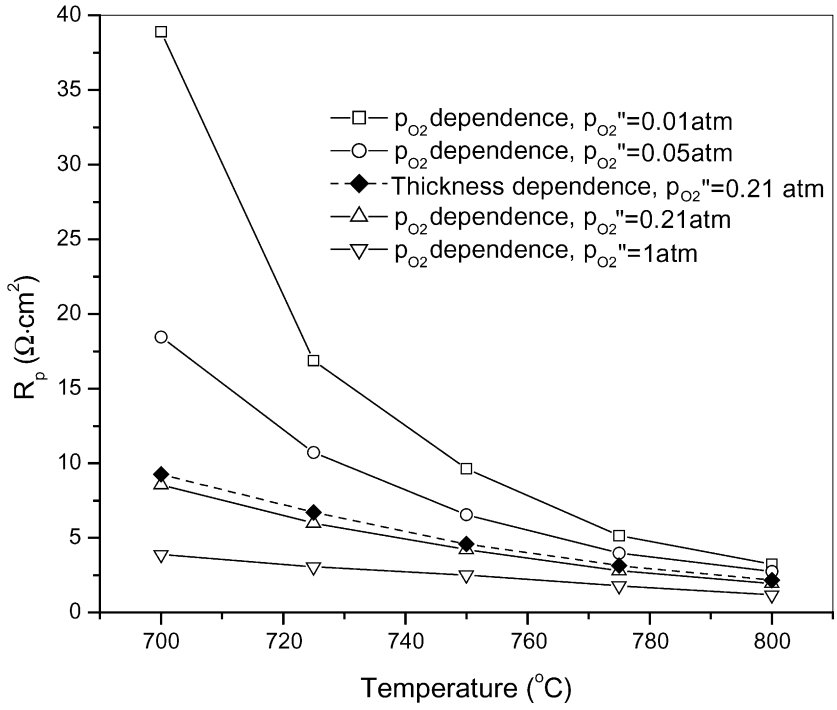

Fig. 8. Overall interfacial resistances determined from the oxygen partial pressure dependence and from the thickness dependence.

than 10%, indicating that the experimental errors are still significant.

4. Conclusions

The dependence of oxygen permeation rate on membrane thickness and on partial pressure of oxygen were used to determine the ionic conductivities and the interfacial resistances of $Sr_{0.25}Bi_{0.5}FeO_{3-\delta}$ at temperatures from 700 to 800 °C. The interfacial resistance primarily limits the oxygen permeability of the SBF membranes at 700 to 800 °C and at low oxygen partial pressures. Thus, adding a catalytically active layer on the surface of the SBF membranes would enhance the oxygen permeability under these conditions.

Acknowledgements

We gratefully acknowledge partial support of this research by National Science Foundation under Award No. CTS-9819850 and by the Georgia Institute of Technology Molecular Design Institute, under prime contract N00014-95-1-1116 from the Office of Naval Research.

References

[1] H.J.M. Bouwmeester, A.J. Burgraaf, in: A.J. Burgraaf, L. Cot (Eds.), Fundamentals of Inorganic Membrane Science and Technology, Elsevier, Amsterdam, 1996, p. 435.
[2] M. Liu, J. Winnick, Solid State Ionics 118 (1999) 11.
[3] S. Aasland, IlL. Tangen, K. Wiik, R. Ødegård, Solid State Ionics 135 (2000) 713.
[4] B. Ma, J.P. Hodges, J.D. Jorgensen, D.J. Miller, J.W. Richardson Jr., U. Balachandran, J. Solid State Chem. 141 (1998) 576.
[5] H.J.M. Bouwmeester, A.J. Burggraaf, in: P.J. Gellings, H.J.M. Bouwmeester (Eds.), CRC Handbook of Solid State Electrochemistry, CRC Press, Boca Raton, FL, 1997, p. 481, Chap. 14.
[6] S. Wang, X. Lu, M. Liu, J. Solid State Electrochem. 5 (6) (2001) 375.
[7] X. Lu, M. Liu, Electrochem. Solid-State Lett. 2 (1999) 452.
[8] T.J. Mazanec, T.L. Cable, J.G. Frye Jr., Solid State Ionics 53–56 (1992) 111.
[9] U. Balachandran, P.S. Maiya, B. Ma, J.T. Dusek, R.L. Mieville, J.J. Picciolo, in: R. Bredesen (Ed.), Proceedings of the 4th Workshop on Catalytic Membrane Reactors, Oslo, Norway, May 30–31, 1997, p. 15.
[10] M. Liu, A. Joshi, in: T.A. Ramanarayanan, H.L. Tuller (Eds.), Proc. 1st International Symp. on Ionic and Mixed Conducting Ceramics,The Electrochemical Society, Pennington, NJ, 91-12, 1991, p. 231.
[11] S. Li, W. Yang, L. Fang, L. Lin, J. Solid State Chem. 130 (1997) 316.
[12] H. Ullmann, N. Trofimenko, Solid State Ionics 119 (1999) 1.